catalysts

MDPI

Article

Improvement of Photocatalytic H_2-Generation under Visible Light Irradiation by Controlling the Band Gap of $ZnIn_2S_4$ with Cu and In

Ikki Tateishi [1,*], Mai Furukawa [2], Hideyuki Katsumata [2] and Satoshi Kaneco [1,2]

1 Global Environment Center for Education & Research, Mie University, Mie 514-8507, Japan
2 Department of Chemistry for Materials, Graduate School of Engineering, Mie University, Mie 514-8507, Japan
* Correspondence: tateishi@gecer.mie-u.ac.jp; Tel.: +81-59-231-9647

Received: 12 July 2019; Accepted: 6 August 2019; Published: 10 August 2019

Abstract: The band gap controlled photocatalyst ($Zn_{0.74}Cu_{0.13}In_2S_{3.805}$) was prepared via a simple one-step solvothermal method. The effects of doping of Cu^+ and excess In on the photocatalytic activity of $ZnIn_2S_4$ photocatalyst were investigated. In addition, optical properties, surface morphology and crystal structure were evaluated. The maximum H_2 evolution rate (2370 μmol h^{-1} g^{-1}) was achieved with $Zn_{0.74}Cu_{0.13}In_2S_{3.805}$, which was about five times higher than that of untreated $ZnIn_2S_4$ under visible light ($\lambda \geq 420$ nm). The band gap of $Zn_{0.74}Cu_{0.13}In_2S_{3.805}$ decreased to 1.98 eV by raising the maximum position of the valence band, compared to $ZnIn_2S_4$. Furthermore, the recombination of electron hole pairs was effectively reduced. This research contributes to the development of highly active photocatalysts under visible light.

Keywords: photocatalytic hydrogen generation; copper; indium; $ZnIn_2S_4$

1. Introduction

Hydrogen is one of the more demanded synthetic energy carriers. Until now, hydrogen can be produced chemically, thermochemically, biologically, biochemically, biophotochemically, etc. [1–4]. Among these techniques, hydrogen generation by water splitting using a photocatalyst has been expected as a clean and sustainable energy technology, because it can directly convert solar energy into chemical energy by using only water as a raw material [5–7]. It is important to develop highly efficient photocatalysts to replace the current hydrogen generation technology with the photocatalytic water splitting process. Sunlight contains ultraviolet light, visible light and infrared light, and it is ideal to use all the wavelengths when using sunlight. It is known that the wavelength ranges of light, in which the photocatalyst reacts, is dependent on the size of the band gap of the photocatalyst [8–10]. Therefore, photocatalytic activity can be exhibited even under longer wavelength light [11–13]. The addition of foreign elements, which is one of the ways to change photocatalytic ability, greatly affects the characteristics of the catalyst. Specific requirements to improve the activity of the photocatalytic material generally include efficient light absorption, effective separation of photogenerated charge carriers, and better efficiency of the interface for direct release of hydrogen and/or oxygen from water [14–16]. In efficient light absorption, the size of the band gap formed by the conduction band (CB) and the valence band (VB) of the semiconductor photocatalyst is the most important issue [17–19]. With regard to the effective separation of photogenerated charge carriers, many elements such as defects in the crystal structure and band structure are involved in a complex manner [20–22].

Sulfide photocatalysts are advantageous for visible light driven photocatalysts, because they have narrow band gaps and negative valence bands due to the electron orbit of S, compared to oxide based photocatalysts [23–25]. $ZnIn_2S_4$ has been tested to have a suitable band gap

corresponding to the visible-light absorption region, high photocatalytic activity and considerable chemical stability for photocatalytic H_2 evolution [26–28]. Yao et al. described the fabrication of Z-scheme PtS–$ZnIn_2S_4$/WO_3-MnO_2 for overall photo-catalytic water splitting [29]. It was reported by Zhao et al. that the combined effects of octahedron NH_2-UiO-66 and flowerlike $ZnIn_2S_4$ microspheres for photocatalytic hydrogen evolution [30]. However, the absorption wavelength of pure $ZnIn_2S_4$ is limited to about 500 nm. Cu species such as Cu^+ and Cu^{2+} affected the valence band of $ZnIn_2S_4$ and formed an advantageous band structure for photocatalysts [31–33]. In In-Zn-S compounds, the $[Zn^{2+}]/[In^{3+}]$ ratio changes the structural and optoelectronic properties, and greatly affects the composition of In–Zn–S [34]. Thus far, there are few reports that $ZnIn_2S_4$ is co-doped with Cu^+ and excess indium. In this study, we investigated photocatalytic activity, optical properties and surface morphology of $ZnIn_2S_4$ simultaneously doped with Cu^+ and excess indium.

2. Results and Discussion

2.1. Structural Characterization

The XRD patterns of $ZnIn_2S_4$, $Zn_{0.87}Cu_{0.13}In_2S_{3.935}$, $Zn_{0.87}In_2S_{3.87}$ and $Zn_{0.74}Cu_{0.13}In_2S_{3.805}$ are shown in Figure 1. The XRD pattern of $ZnIn_2S_4$ could be indexed as the hexagonal structure (JCPDS No. 65-2023). The three diffraction peaks at around 20.8°, 27.5°, 47.2° and 56.4° could be assigned to the (006), (101), (110) and (202) planes, respectively [35,36]. The XRD patterns of other $Zn_{0.87}Cu_{0.13}In_2S_{3.935}$, $Zn_{0.87}In_2S_{3.87}$ and $Zn_{0.74}Cu_{0.13}In_2S_{3.805}$ photocatalysts also showed similar results. These XRD patterns were in agreement with those reported in previous studies [35], which revealed that $Zn_{0.74}Cu_{0.13}In_2S_{3.805}$ is a hexagonal structure and contains almost no impurities of ZnS. The reason that the Cu and In derived peaks were not observed could be due to the very low doping amount. In addition, with respect to the peak of the (006) plane, a slight shift toward the high angle was observed when doping Cu and increasing In. This means that the interplanar spacing was reduced by doping, suggesting that Cu and excess In may be incorporated into the crystal structure of $ZnIn_2S_4$ and exist as a solid solution.

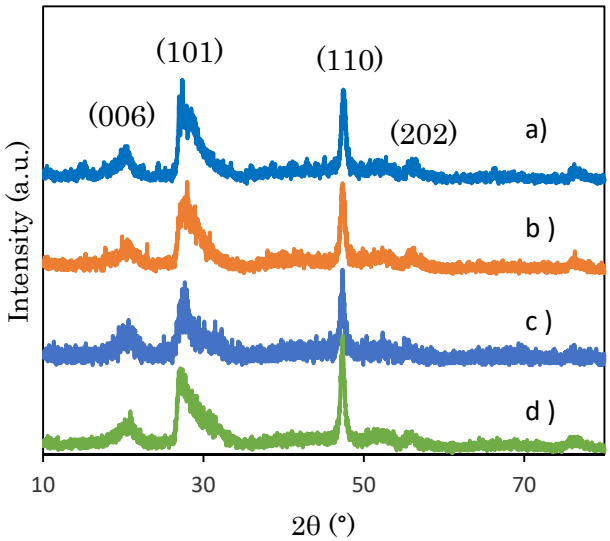

Figure 1. XRD patterns of (**a**) $ZnIn_2S_4$, (**b**) $Zn_{0.87}In_2S_{3.87}$, (**c**) $Zn_{0.87}Cu_{0.13}In_2S_{3.935}$ and (**d**) $Zn_{0.74}Cu_{0.13}In_2S_{3.805}$.

The results of the X-ray photoelectron spectroscopy (XPS) measurement for further structural analysis of photocatalysts are shown in Figure 2. The elemental ratios determined from the XPS spectrum are shown in Table S2. XPS survey spectra of $Zn_{0.87}In_2S_{3.87}$, $Zn_{0.87}Cu_{0.13}In_2S_{3.935}$ and $Zn_{0.74}Cu_{0.13}In_2S_{3.805}$ matched the material $ZnIn_2S_4$. This indicates that the impurities were not contained regardless of the doping Cu^+ and excess In. Furthermore, from the result of elemental

ratio analysis of XPS, it could be confirmed that the elemental ratio of the prepared catalysts were substantially in agreement with the theoretical ratio. Typical narrow spectra of $Zn_{0.74}Cu_{0.13}In_2S_{3.805}$ are shown in Figure 2a. In the XPS spectrum of Zn 2p, the peak of Zn $2p_{3/2}$ (1020.4 eV) was observed. This peak was derived from the $ZnIn_2S_4$ component in $Zn_{0.74}Cu_{0.13}In_2S_{3.805}$. In the XPS spectrum of In 3d from $ZnIn_2S_4$ and In_2S_3, binding energies of 443.7 (In $3d_{5/2}$) and 451.0 eV (In $3d_{3/2}$) were observed. The peaks of S 2p were at 161.3 eV (S $2p_{3/2}$) and 162.6 eV (S $2p_{1/2}$) [37,38]. In addition, since the peak position of Cu $2p_{3/2}$ is observed only at 932 eV and Cu $2p_{3/2}$ satellite peak derived from Cu^{2+} was not present at 942 eV, it can be seen that Cu was doped in a monovalent state [39,40]. Both results of XRD and XPS show that the basic structure of $Zn_{0.74}Cu_{0.13}In_2S_{3.805}$ is hexagonal $ZnIn_2S_4$, doped with Cu^+ and excess In.

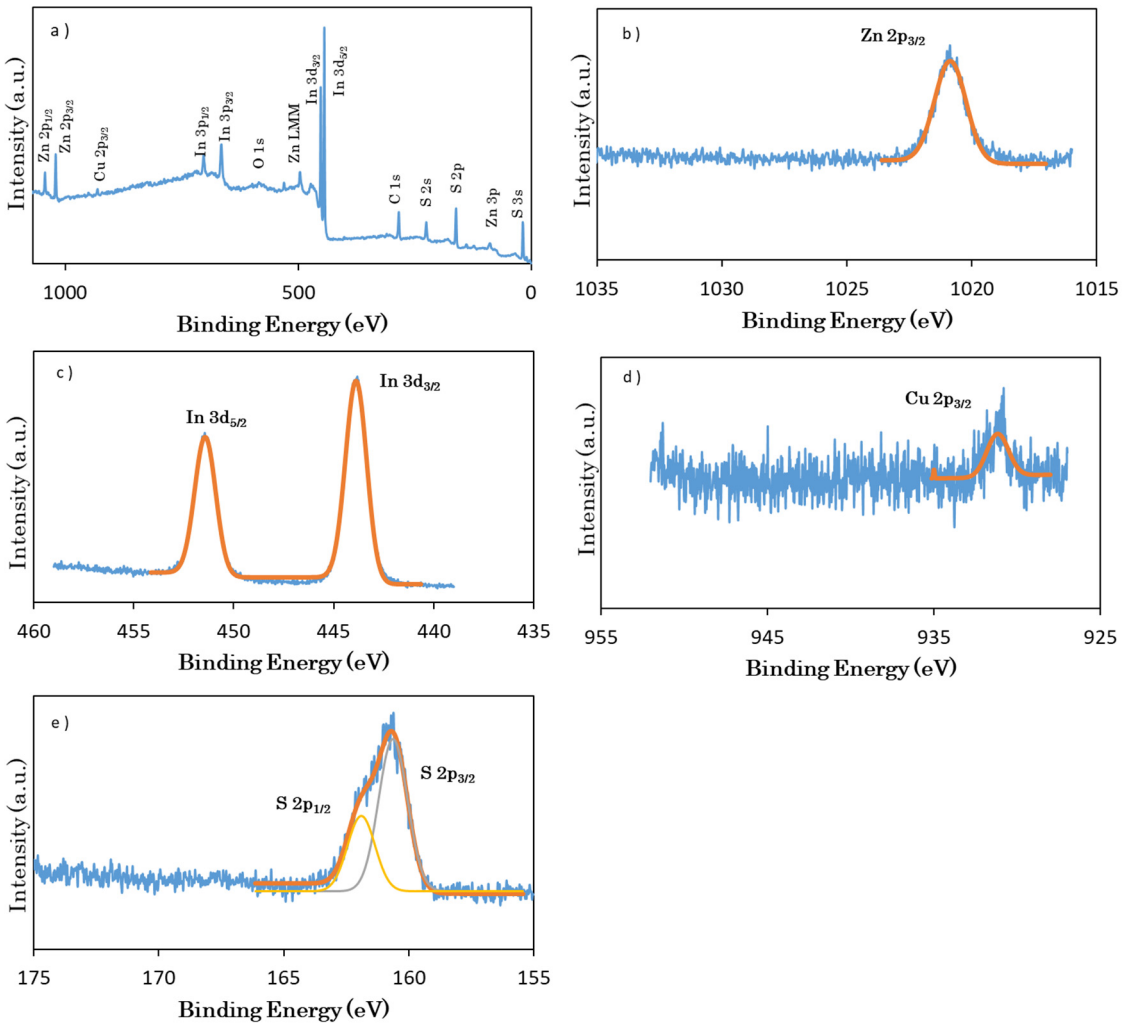

Figure 2. X-ray photoelectron spectroscopy (XPS) narrow and survey spectra of $Zn_{0.74}Cu_{0.13}In_2S_{3.805}$. (**a**) survey, (**b**) Zn, (**c**) In, (**d**) Cu and (**e**) S.

2.2. Morphological Analysis

In order to investigate the influence of Cu and excess In doping on the characteristic surface morphology, SEM images of the prepared photocatalysts were observed. The results are shown in Figure 3. In pure $ZnIn_2S_4$, a microsphere structure formed by the overlapping of nanosheets was observed [41]. When Cu and excess In was doped, the spherical structure was destroyed. The nanosheet structure also collapsed and aggregated. The shapes of pure $ZnIn_2S_4$ and $Zn_{0.74}Cu_{0.13}In_2S_{3.805}$ were very different. Maybe, Cu^+ and excess In formed a solid solution with $ZnIn_2S_4$.

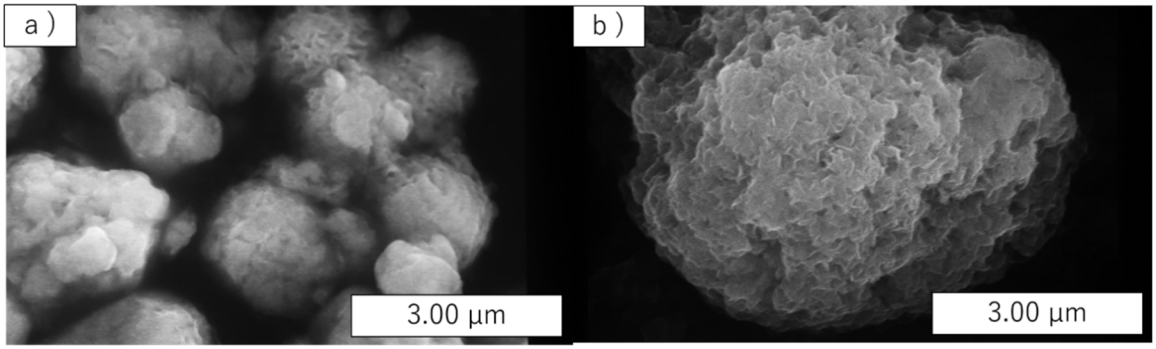

Figure 3. SEM images of (**a**) $ZnIn_2S_4$ and (**b**) $Zn_{0.74}Cu_{0.13}In_2S_{3.805}$.

2.3. Optical Analysis

Figure 4 shows the absorption wavelength region of light using the UV-visible diffuse reflectance spectrum. Furthermore, a Tauc plot calculated from the UV-vis diffuse reflectance spectra (DRS) spectrum is shown in Figure S1, in order to obtain a band gap. As shown in the results of DRS and Tauc plot, the absorption edge of pure $ZnIn_2S_4$ was 480 nm, and the size of the band gap was 2.67 eV. When $[Zn^{2+}]/[In^{3+}]$ mole ratio was changed ($Zn_{0.87}In_2S_{3.87}$), the absorption tendencies were almost similar to $ZnIn_2S_4$. However, when Cu^+ doping ($Zn_{0.87}Cu_{0.13}In_2S_{3.935}$) and excess In doping ($Zn_{0.74}Cu_{0.13}In_2S_{3.805}$) were performed, the absorption edges were extended to about 700 nm. Consequently, the band gap of $ZnIn_2S_4$ similarly decreased in the case of the doping Cu and excess In. So as to analyze the band structure, valence band edge measurement for the prepared photocatalysts was performed by XPS. It is clear from the results in Figure S2 that the doping of Cu^+ shifted the valence band edge to the negative side. It has been reported that the doping of In^{3+} forms a sub-band on the positive side of the conduction band of $ZnIn_2S_4$ [36]. Therefore, it is reasonable that the doping of Cu^+ and In into the photocatalyst reduce the band gap energy of $ZnIn_2S_4$.

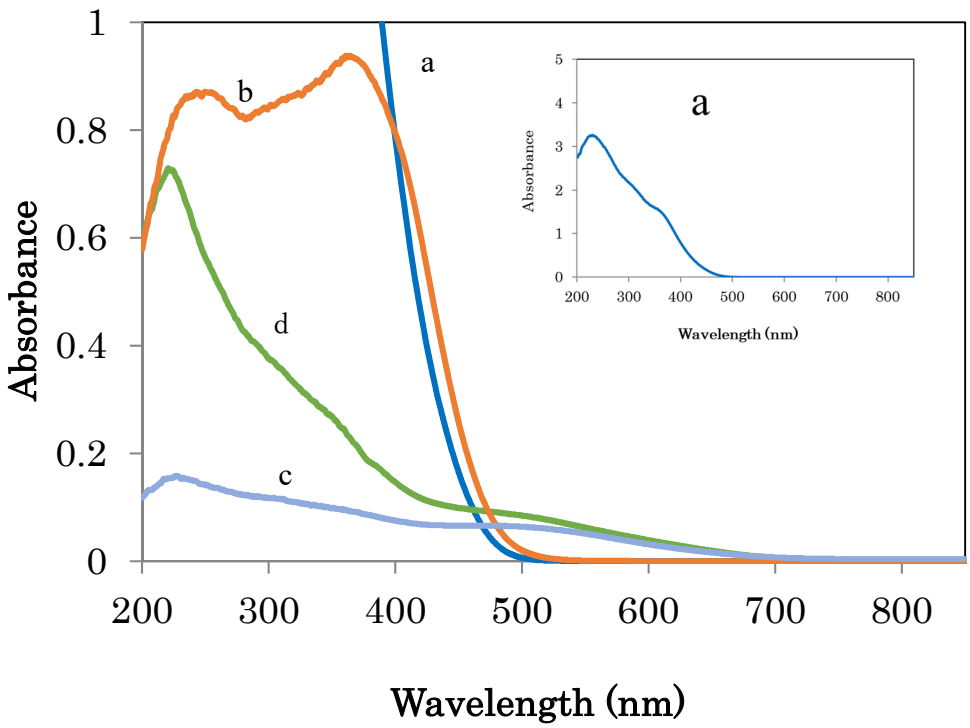

Figure 4. UV-visible spectra of (**a**) $ZnIn_2S_4$, (**b**) $Zn_{0.87}In_2S_{3.87}$, (**c**) $Zn_{0.87}Cu_{0.13}In_2S_{3.935}$ and (**d**) $Zn_{0.74}Cu_{0.13}In_2S_{3.805}$.

We investigated the photoluminescence spectra in order to investigate the electron–hole pair separation efficiency, and the results are shown in Figure 5. Luminescence in ultraviolet and visible regions was observed in the photoluminescence spectrum. In general, ultraviolet emission is associated with exciton transition and recombination from the conduction band level to the valence band, and visible light emission is mainly associated with intrinsic or extrinsic defects in the catalyst. The photoluminescence spectra of $ZnIn_2S_4$ was approximately close to $Zn_{0.87}In_2S_{3.87}$. On the other hand, the spectra from $Zn_{0.87}Cu_{0.13}In_2S_{3.935}$ and $Zn_{0.74}Cu_{0.13}In_2S_{3.805}$ were lowered by doping of Cu^+ and excess In. This may have been due to the decrease of the recombination rate between the photogenerated holes and the electrons photogenerated in the valence band. The photogenerated electrons may have been trapped in the oxygen vacancies generated in the photocatalyst by doping.

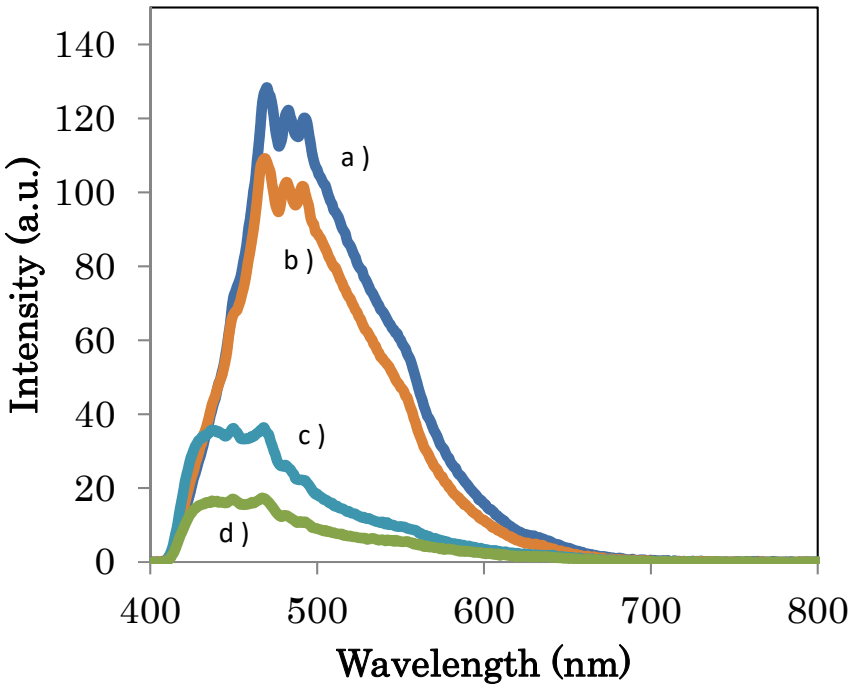

Figure 5. Photoluminescence spectra for (**a**) $ZnIn_2S_4$, (**b**) $Zn_{0.87}In_2S_{3.87}$, (**c**) $Zn_{0.87}Cu_{0.13}In_2S_{3.935}$ and (**d**) $Zn_{0.74}Cu_{0.13}In_2S_{3.805}$. Excitation: 350 nm.

2.4. Photocatalytic Activity

Hydrogen generation was conducted using the photocatalyst $Zn_{0.74}Cu_{0.13}In_2S_{3.805}$. $ZnIn_2S_4$, $Zn_{0.87}In_2S_{3.87}$ and $Zn_{0.87}Cu_{0.13}In_2S_{3.935}$ were used as comparative objects. All catalysts were loaded with 1wt% Pt as a cocatalyst. The results are shown in Figure 6. The photocatalyst $ZnIn_2S_4$ mono-doped with excess In showed slightly higher hydrogen generation activity than that of pure $ZnIn_2S_4$. On the other hand, $ZnIn_2S_4$ doped only with Cu^+ greatly improved the photocatalytic activity. Furthermore, the photocatalyst doped with Cu^+ and excess In showed the highest hydrogen generation activity. The maximum H_2 evolution rate was 2370 μmol h^{-1} g^{-1}, which showed about five times better results than that of untreated $ZnIn_2S_4$. The reproducibility of the H_2 production (relative standard deviation (RSD), for hydrogen amounts) was better than RSD 4% for three repeated measurements.

The TEM images before and after the hydrogen generation of $Zn_{0.74}Cu_{0.13}In_2S_{3.805}$ photocatalyst are shown in Figure S3. Only after hydrogen generation, a 3–4 nm spot was observed on the sample surface. The spot deposition was Pt, which was reduced during the hydrogen production.

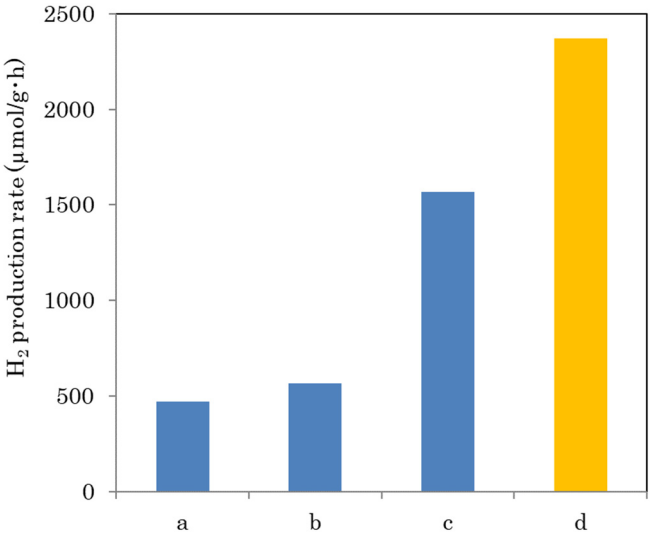

Figure 6. Photocatalytic hydrogen production rate with (**a**) $ZnIn_2S_4$, (**b**) $Zn_{0.87}In_2S_{3.87}$, (**c**) $Zn_{0.87}Cu_{0.13}In_2S_{3.935}$ and (**d**) $Zn_{0.74}Cu_{0.13}In_2S_{3.805}$.

2.5. Proposed Hydrogenation Mechanism

The reaction mechanism is shown in Scheme 1. Irradiation of light having a wavelength corresponding to the band gap energy of the $Zn_{0.74}Cu_{0.13}In_2S_{3.805}$ photocatalyst excites electrons in the valence band to the conduction band to produce an electron–hole pair (Formula (1)). From the results of DRS and photoluminescence (PL), it could be considered that Cu^+ and excess In doping enhanced charge separation by forming an impurity level on the negative side of the valence band of $ZnIn_2S_4$ and the positive side of the conduction band, narrowing the band gap. In Formula (2), a part of electrons excited in the conduction band is consumed for photodeposition of Pt. The deposited Pt reduces H^+ by using electrons transferred from the photocatalyst to generate H_2 (Formula (3)). On the other hand, sulfite ions and sulfide ions consume the holes for promoting a hydrogen generation reaction. The presence of Na_2S is very important in enhancing the photocatalytic activity, as Na_2S stabilizes the surface of the metal sulfide by suppressing the formation of surface defects as a scavenger of holes. However, when the concentration of Na_2S is high, the pH becomes high. High pH values are thermodynamically disadvantageous in the reaction represented by Formula (4). As described in the Formulas (5)–(7), SO_3^{2-} and S^{2-} consume holes. According to the Formula (6), S_2^{2-} ions are generated and act as an optical filter. If S_2^{2-} is not consumed, it interferes with light absorption. As shown in Formula (8), the reaction between S_2^{2-} and SO_3^{2-} forms $S_2O_3^{2-}$, which is colorless and can hardly affect to light absorption.

$$\text{Photocatalyst} + h\nu \rightarrow e^- + h^+ \quad (1)$$

$$Pt^{2+} + 2e^-_{CB} \rightarrow Pt \quad (2)$$

$$2H^+ + 2e^-_{CB} \rightarrow H_2 \quad (3)$$

$$2H_2O + 2e^-_{CB} \rightarrow H_2 + 2OH^- \quad (4)$$

$$SO_3^{2-} + H_2O + 2h^+_{VB} \rightarrow SO_4^{2-} + 2H^+ \quad (5)$$

$$2S^{2-} + 2h^+_{VB} \rightarrow S_2^{2-} \quad (6)$$

$$SO_3^{2-} + S^{2-} + 2h^+_{VB} \rightarrow S_2O_3^{2-} \quad (7)$$

$$S_2^{2-} + SO_3^{2-} \rightarrow S_2O_3^{2-} + S^{2-} \quad (8)$$

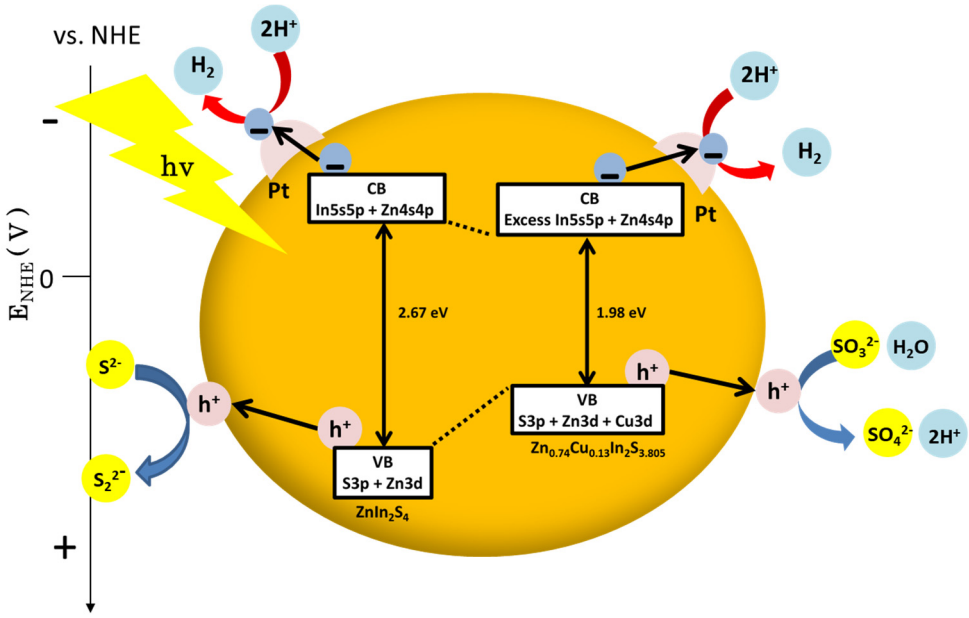

Scheme 1. H_2 production mechanism.

3. Materials and Methods

3.1. Preparation of Photocatalysts

All chemicals were analytical grade and used as received without further purification. $Zn_{0.74}Cu_{0.13}In_2S_{3.805}$ was prepared by a simple hydrothermal method. Cetyltrimethylammonium bromide (CTAB, 3.76 mmol) (Wako Pure Chemical Industries, Ltd., Osaka, Japan), stoichiometric mole of $ZnSO_4{\cdot}7H_2O$ (Nacalai Tesque, Inc., Kyoto, Japan), $InCl_3{\cdot}4H_2O$ and CuCl (I) and an excess of thioacetamide (TAA) (Wako Pure Chemical Industries, Ltd., Osaka, Japan) were dissolved in 50 mL of distilled water. At the same time, in order to keep Cu monovalent, nitrogen was purged into the solution for 10 min to remove dissolved oxygen. The mixed solution was then transferred into a 100 mL Teflon autoclave. The autoclave was sealed, kept at 160 °C for 1 h and cooled to room temperature naturally. After cooling, the product was dried in a vacuum at 40 °C for 4 h and was ground for 30 min. $ZnIn_2S_4$ (not doped), $Zn_{0.87}Cu_{0.13}In_2S_{3.935}$ (Cu^+ doped) and $Zn_{0.87}In_2S_{3.87}$ (change of Zn^{2+}/In^{3+}) were also prepared by the same method as reference materials. The prepared photocatalysts are shown in F1.

3.2. Characterization of Samples

X-ray powder diffraction (XRD) measurements were performed using a Rigaku RINT Ultima-IV diffractometer. It was carried out by using Cu radiation at a scan rate of 0.04°/s in a scan range of 10°–80°. X-ray photoelectron spectroscopy (XPS) measurements were carried out with a PHI Quantera SXM photoelectron spectrometer using Al Kα radiation. To compensate for surface charge effects, binding energies were calibrated using the C1s peak at 284 eV as the reference. Scanning electron microscope (SEM) observations were performed using a Hitachi S-4000 SEM. The transmission electron microscopy (TEM) images were taken on JEOL product JEM1011. The UV–vis diffuse reflectance spectra (DRS) of the photocatalysts were recorded using a Shimadzu UV-2450 spectrophotometer equipped with an integral sphere assembly, using $BaSO_4$ as a reflectance standard. Photoluminescence (PL) spectra were obtained at an excitation wavelength of 350 nm by using a Shimadzu RF-5300PC spectrofluorophotometer.

3.3. Photocatalytic Hydrogen Generation

A Pyrex column vessel reactor (inner volume: 123 mL) was used for the photocatalytic production of hydrogen from aqueous sulfide solution. In all experiments, 40 mL of solution containing 40 mg of catalyst, 10 mL of 0.04 ppm H_2PtCl_6 solution and 0.25 M Na_2SO_3/0.35 M Na_2S mixed sacrificial

agent was added into the reaction cell. The light source was a 4000–4500 μW/cm^2 Xe-lamp (300 W), with a cut-off filter (λ ≥ 420 nm). Nitrogen was purged into the system for 30 min before the reaction to remove oxygen. The concentrations of H_2 were measured with an online gas chromatograph (GC). Injection, column and detector in GC were 50 °C. A thermal conductivity detector (TCD) was used as detector. The hydrogen generation experimental conditions are shown in Table 1.

Table 1. Hydrogen generation experimental conditions.

Photocatalyst	$ZnIn_2S_4$, $Zn_{0.87}In_2S_{3.87}$, $Zn_{0.87}Cu_{0.13}In_2S_{3.935}$, $Zn_{0.74}Cu_{0.13}In_2S_{3.805}$
Cocatalyst	0.04 ppm H_2PtCl_6 10 mL (1.0 wt%)
Medium	0.25 M Na_2SO_3 / 0.35 M Na_2S 40 mL
Reactor	Pyrex glass vessel (volume: 123 mL)
Temperature	Room temperature (25 °C)
Light source	Xenon lamp (λ ≥ 420 nm, 4500 μW/cm^2)
Irradiation time	6 h
Analysis	Gas chromatography (TCD)

4. Conclusions

The $Zn_{0.74}Cu_{0.13}In_2S_{3.805}$ photocatalyst, in which $ZnIn_2S_4$ was doped with Cu^+ and excess In, was prepared by a simple one-pot solvothermal method. From the SEM, XRD and XPS results, it is highly possible that $Zn_{0.74}Cu_{0.13}In_2S_{3.805}$ is a solid solution with a hexagonal $ZnIn_2S_4$ as a basic structure. Control of the band gap and suppression of electron–hole recombination were confirmed by doping $ZnIn_2S_4$ with Cu^+ and excess In. In addition, an increase in the absorption wavelength range and improved catalytic activity were observed. The hydrogen generation rate by $Zn_{0.74}Cu_{0.13}In_2S_{3.805}$ was 2370 μmol g^{-1} h^{-1}, which was almost five times larger compared with that obtained with $ZnIn_2S_4$. The present work provides a strategy for water splitting systems consisting of sulfide materials with narrow band gaps for efficient hydrogen production.

Supplementary Materials: The following are available online at http://www.mdpi.com/2073-4344/9/8/681/s1. Table S1: Expected composite components of photocatalyst (molar ratio), Table S2: Elemental ratios of $ZnIn_2S_4$, $Zn_{0.87}In_2S_{3.87}$, $Zn_{0.87}Cu_{0.13}In_2S_{3.935}$ and $Zn_{0.74}Cu_{0.13}In_2S_{3.805}$ from XPS results, Figure S1: Tauc plots of (a) $ZnIn_2S_4$, (b) $Zn_{0.87}In_2S_{3.87}$, (c) $Zn_{0.87}Cu_{0.13}In_2S_{3.935}$ and (d) $Zn_{0.74}Cu_{0.13}In_2S_{3.805}$, Figure S2: Valence-band XPS spectra of (a) $ZnIn_2S_4$, (b) $Zn_{0.87}In_2S_{3.87}$, (c) $Zn_{0.87}Cu_{0.13}In_2S_{3.935}$ and (d) $Zn_{0.74}Cu_{0.13}In_2S_{3.805}$, Figure S3: TEM images of $Zn_{0.74}Cu_{0.13}In_2S_{3.805}$ (a) before and (b) after irradiation.

Author Contributions: I.T. and H.K. conceived and designed the experiments. I.T. performed the experiments and wrote the paper. I.T., M.F., S.K. and H.K. analyzed the results and advised the project.

Funding: This research received no external funding.

Note: All experiments were conducted at Mie University. Any opinions, findings, conclusions or recommendations expressed in this paper are those of the authors and do not necessarily reflect the view of the supporting organizations.

Conflicts of Interest: The authors declare no conflict of interest.

References

1. Skoplyak, O.; Barteau, M.A.; Chen, J.G.G. Comparison of H_2 production from ethanol and ethylene glycol on M/Pt(1 1 1) (M = Ni, Fe, Ti) bimetallic surfaces. *Catal. Today* **2009**, *147*, 150–157. [CrossRef]
2. Barthos, R.; Sze'chenyi, A.; Solymos, F. Efficient H_2 Production from Ethanol over Mo_2 C/C Nanotube Catalyst. *Catal. Lett.* **2008**, *120*, 161–165. [CrossRef]
3. Baamran, K.S.; Tahir, M. Thermodynamic investigation and experimental analysis on phenol steam reforming towards enhanced H_2 production over structured Ni/$ZnTiO_3$ nanocatalyst. *Energy Convers. Manag.* **2019**, *180*, 796–810. [CrossRef]
4. Politano, A.; Cattelan, M.; Boukhvalov, D.W.; Campi, D.; Cupolillo, A.; Agnoli, S.; Apostol, N.G.; Lacovig, P.; Lizzit, S.; Farías, D. Unveiling the Mechanisms Leading to H_2 Production Promoted by Water Decomposition on Epitaxial Graphene at Room Temperature. *ACS Nano* **2016**, *10*, 4543–4549. [CrossRef] [PubMed]

5. Kudo, A. Development of photocatalyst materials for water splitting. *Int. J. Hydrogen Energy* **2006**, *31*, 197–202. [CrossRef]
6. Kato, H.; Kudo, A. Photocatalytic water splitting into H_2 and O_2 over various tantalate photocatalysts. *Catal. Today* **2003**, *78*, 561–569. [CrossRef]
7. Chen, X.; Shen, S.; Guo, L.; Mao, S.S. Semiconductor-based Photocatalytic Hydrogen Generation. *Chem. Rev.* **2010**, *110*, 6503–6570. [CrossRef]
8. Tsuji, I.; Kato, H.; Kobayashi, H.; Kudo, A. Photocatalytic H_2 evolution reaction from aqueous solutions over band structure-controlled $(AgIn)_xZn_{2(1-x)}S_2$ solid solution photocatalysts with visible-light response and their surface nanostructures. *J. Am. Chem. Soc.* **2004**, *126*, 13406–13413. [CrossRef]
9. Peng, S.; Zhu, P.; Thavasi, V.; Mhaisalkar, S.G.; Ramakrishna, S. Facile solution deposition of $ZnIn_2S_4$ nanosheet films on FTO substrates for photoelectric application. *Nanoscale* **2011**, *3*, 2602–2608. [CrossRef]
10. Zhang, X.; Yu, L.; Zhuang, C.; Peng, T.; Li, R.; Li, X. Highly Asymmetric Phthalocyanine as a Sensitizer of Graphitic Carbon Nitride for Extremely Efficient Photocatalytic H_2 Production under Near-Infrared Light. *ACS Catal.* **2014**, *4*, 162–170. [CrossRef]
11. Dai, W.W.; Zhao, Z.Y. DFT study on the interfacial properties of vertical and in-plane $BiOI/BiOIO_3$ hetero-structures, Phys. Chem. *Chem. Phys.* **2017**, *19*, 9900–9911.
12. Vaiano, V.; Iervolino, G.; Rizzo, L. Cu-doped ZnO as efficient photocatalyst for the oxidation of arsenite to arsenate under visible light. *Appl. Catal. B* **2018**, *238*, 471–479. [CrossRef]
13. Shafaee, M.; Goharshadi, E.K.; Mashreghi, M.; Sadeghinia, M. TiO_2 nanoparticles and TiO_2@graphene quantum dots nancomposites as effective visible/solar light photocatalysts. *J. Photochem. Photobiol. A Chem.* **2018**, *357*, 90–102. [CrossRef]
14. Chang, C.J.; Wang, C.W.; Wei, Y.H.; Chen, C.Y. Enhanced photocatalytic H_2 production activity of Ag-doped Bi_2WO_6-graphene based photocatalysts. *Int. J. Hydrogen Energy* **2018**, *43*, 11345–11354. [CrossRef]
15. Jia, Y.; Zhao, D.; Li, M.; Han, H.; Li, C. La and Cr Co-doped $SrTiO_3$ as an H_2 evolution photocatalyst for construction of a Z-scheme overall water splitting system. *Chin. J Catal.* **2018**, *39*, 421–430. [CrossRef]
16. Yan, X.; Xue, C.; Yang, B.; Yang, G. Novel three-dimensionally ordered macroporous Fe^{3+}-doped TiO_2 photocatalysts for H_2 production and degradation applications. *Appl. Surf. Sci.* **2017**, *394*, 248–257. [CrossRef]
17. Singh, J.; Sharma, S.; Sharma, S.; Chand Singh, R. Effect of tungsten doping on structural and optical properties of rutile TiO_2 and band gap narrowing. *Optik* **2019**, *182*, 538–547. [CrossRef]
18. Sharma, P.K.; Cortes, M.A.L.R.M.; Hamilton, J.W.J.; Han, Y.; Byrne, J.A.; Nolan, M. Surface modification of TiO_2 with copper clusters for band gap narrowing. *Catal. Today* **2018**, *321–322*, 9–17. [CrossRef]
19. Liu, C.; Chai, B.; Wang, C.; Yan, J.; Ren, Z. Solvothermal fabrication of MoS_2 anchored on $ZnIn_2S_4$ microspheres with boosted photocatalytic hydrogen evolution activity. *Int. J. Hydrogen Energy* **2018**, *43*, 6977–6986. [CrossRef]
20. Gao, P.; Li, A.; Sun, D.D.; Ng, W.J. Effects of various TiO_2 nanostructures and graphene oxide on photocatalytic activity of TiO_2. *J. Hazard. Mater.* **2014**, *279*, 96–104. [CrossRef]
21. Guo, J.; Liao, X.; Lee, M.-H.; Hyett, G.; Huang, C.C.; Hewak, D.W.; Mails, S.; Zhou, W.; Jiang, Z. Experimental and DFT insights of the Zn-doping effects on the visible-light photocatalytic water splitting and dye decomposition over Zn-doped BiOBr photocatalysts. *Appl. Catal. B* **2019**, *243*, 502–512. [CrossRef]
22. Behzadifard, Z.; Shariatinia, Z.; Jourshabani, M. Novel visible light driven $CuO/SmFeO_3$ nanocomposite photocatalysts with enhanced photocatalytic activities for degradation of organic pollutants. *J. Mol. Liq.* **2018**, *262*, 533–548. [CrossRef]
23. Li, T.L.; Cai, C.D.; Yeh, T.F.; Teng, H. Capped $CuInS_2$ quantum dots for H_2 evolution from water under visible light illumination. *J. Alloys Compd.* **2013**, *550*, 326–330. [CrossRef]
24. You, D.; Pan, B.; Jiang, F.; Zhou, Y.; Su, W. CdS nanoparticles/CeO_2 nanorods composite with high-efficiency visible-light-driven photocatalytic activity. *Appl. Surf. Sci.* **2016**, *363*, 154–160. [CrossRef]
25. Jin, X.; Chen, F.; Jia, D.; Cao, Y.; Duan, H.; Long, M.; Yang, L. Influences of synthetic conditions on the photocatalytic performance of ZnS/graphene composites. *J. Alloys Compd.* **2019**, *780*, 299–305. [CrossRef]
26. Zhang, S.; Wang, L.; Liu, C.; Luo, J.; Crittenden, J.; Liu, X.; Ca, T.; Yuan, J.; Pei, Y.; Liu, Y. Photocatalytic wastewater purification with simultaneous hydrogen production using MoS_2 QD-decorated hierarchical assembly of $ZnIn_2S_4$ on reduced graphene oxide photocatalyst. *Water Res.* **2017**, *121*, 11–19. [CrossRef]

27. Fan, B.; Chen, Z.H.; Liu, Q.; Zhang, Z.G.; Fang, X.M. One-pot hydrothermal synthesis of Ni-doped $ZnIn_2S_4$ nanostructured film photoelectrodes with enhanced photoelectrochemical performance. *Appl. Surf. Sci.* **2016**, *370*, 252–259. [CrossRef]
28. Ding, Y.; Gao, Y.; Li, Z. Carbon quantum dots (CQDs) and $Co(dmgH)_2PyCl$ synergistically promote photocatalytic hydrogen evolution over hexagonal $ZnIn_2S_4$. *Appl. Surf. Sci.* **2018**, *462*, 255–262. [CrossRef]
29. Ding, Y.; Wei, D.; He, R.; Yuan, R.; Xie, T.; Li, Z. Rational Design of Z-Scheme PtS-$ZnIn_2S_4$/WO_3-MnO_2 for Overall Photo-catalytic Water Splitting under Visible Light. *Appl. Catal. B Environ.* **2019**, *258*, 117948. [CrossRef]
30. Zhao, C.; Zhang, Y.; Jiang, H.; Chen, J.; Liu, Y.; Liang, Q.; Zhou, M.; Li, Z.; Zhou, Y. Combined Effects of Octahedron NH_2-UiO-66 and Flowerlike $ZnIn_2S_4$ Microspheres for Photocatalytic Dye Degradation and Hydrogen Evolution Under Visible Light. *J. Phys. Chem. C* **2019**, *123*, 18037–18049. [CrossRef]
31. Liu, A.; Yu, C.; Lin, J.; Sun, G.; Xu, G.; Huang, Y.; Liu, Z.; Tang, C. Construction of $CuInS_2$@ZIF-8 nanocomposites with enhanced photocatalytic activity and durability. *Mater. Res. Bull.* **2019**, *112*, 147–153. [CrossRef]
32. Shen, S.; Zhao, L.; Zhou, Z.; Guo, L. Enhanced Photocatalytic Hydrogen Evolution over Cu-Doped $ZnIn_2S_4$ under Visible Light Irradiation. *J. Phys. Chem. C* **2008**, *112*, 16148–16155. [CrossRef]
33. Zhang, G.; Zhang, W.; John, C.C.; Chen, Y.; Minakata, D.; Wang, P. Photocatalytic hydrogen production under visible-light irradiation on $(CuAg)_{0.15}In_{0.3}Zn_{1.4}S_2$ systhesized by precipitation and calcination. *Chin. J. Catal.* **2013**, *34*, 1926–1935. [CrossRef]
34. Shen, S.H.; Zhao, L.; Guo, L.J. $ZnmIn_2S_{3+m}$ (m=1–5, integer): A new series of visible-light-driven photocatalysts for splitting water to hydrogen. *Int. J. Hydrogen Energy* **2010**, *35*, 10148–10154. [CrossRef]
35. Sun, M.; Zhao, X.; Zeng, Q.; Yan, T.; Ji, P.G.; Wu, T.T.; Wei, D.; Du, B. Facile synthesis of hierarchical $ZnIn_2S_4$/$CdIn_2S_4$ microspheres with enhanced visible light driven photocatalytic activity. *Appl. Surf. Sci.* **2017**, *407*, 328–336. [CrossRef]
36. Song, K.; Zhu, R.; Tian, F.; Cao, G.; Ouyang, F. Effects of indium contents on photocatalytic performance of $ZnIn_2S_4$ for hydrogen evolution under visible light. *J. Solid State Chem.* **2015**, *232*, 138–143. [CrossRef]
37. Du, C.; Zhang, Q.; Lin, Z.; Yan, B.; Xia, C.; Yang, G. Half-unit-cell ZnIn2S4 monolayer with sulfur vacancies for photocatalytic hydrogen evolution. *Appl. Catal. B.* **2019**, *248*, 193–201. [CrossRef]
38. Yang, X.; Li, Q.; Lv, K.L.; Li, M. Heterojunction construction between TiO_2 hollowsphere and $ZnIn_2S_4$ flower for photocatalysis application. *Appl. Surf. Sci.* **2017**, *398*, 81–88.
39. Yue, W.; Han, S.; Peng, R.; Shen, W.; Geng, H.; Wu, F.; Tao, S.; Wang, M. $CuInS_2$ quantum dots synthesized by a solvothermal route and their application as effective electron acceptors for hybrid solar cells. *J. Mater. Chem.* **2010**, *20*, 7570–7578. [CrossRef]
40. Zepeda, T.A.; Pawelec, B.; Díaz de León, J.N.; de los Reyes, J.A.; Olivas, A. Effect of gallium loading on the hydrodesulfurization activity of unsupported Ga_2S_3/WS_2 catalysts. *Appl. Catal. B* **2012**, *111–112*, 10–19. [CrossRef]
41. Chen, S.; Li, S.; Xiong, L.; Wang, G. In-situ growth of $ZnIn_2S_4$ decorated on electrospun TiO_2 nanofibers with enhanced visible-light photocatalytic activity. *Chem. Phys. Lett.* **2018**, *706*, 68–75. [CrossRef]

© 2019 by the authors. Licensee MDPI, Basel, Switzerland. This article is an open access article distributed under the terms and conditions of the Creative Commons Attribution (CC BY) license (http://creativecommons.org/licenses/by/4.0/).